Progress In Electromagnetics Research B, Vol. 34, 47–61, 2011

DOMINANT FACTORS AFFECTING TEMPERATURE ELEVATION IN ADULT AND CHILD MODELS EXPOSED TO SOLAR RADIATION IN HOT ENVIRONMENT

R. Hanatani [1], I. Laakso [1], A. Hirata [1,*], M. Kojima [2,3,4], and H. Sasaki [2,3]

[1]Department of Computer Science and Engineering, Nagoya Institute of Technology, Nagoya 466-8555, Japan

[2]Division of Vision Research for Environmental Health, Medial Research Institute, Kanazawa Medical University, Ishikawa 920-0293, Japan

[3]Department of Ophthalmology, Kanazawa Medical University, Ishikawa 920-0293, Japan

[4]School of Nursing, Kanazawa Medical University, Ishikawa 920-0293, Japan

Abstract—The number of children suffering from heat-related illness has been increasing in recent years. Children are more susceptible to heat-related illness than adults, which is considered to be caused by morphological and functional differences between adults and children. In the present study, the temperature change and perspiration in adult and child models during a simultaneous exposure to solar radiation and a hot environment are evaluated computationally. First, the power absorbed in the human body due to solar radiation is computed by the FDTD method for the Maxwell equations. Then, the temperature distribution inside the human body is modeled by the bioheat equation taking into account the thermophysiological response. Anatomically-based Japanese adult male and 3-year-old child phantoms are used. An approximative analytical solution for the core temperature elevation is also derived to clarify the dominant factors affecting the temperature elevation. From our computational results, the core temperature elevation in the child phantom for both the solar and hot-environment exposures was larger than that in the adult phantom. The temperature elevation in the child was found to be mainly caused by the exposure

Received 19 July 2011, Accepted 15 August 2011, Scheduled 31 August 2011

* Corresponding author: Akimasa Hirata (ahirata@nitech.ac.jp).

to a hot environmental temperature while that in the adult was due to the environmental heat and solar radiation almost equally. This difference was mainly attributed to the difference in the surface area-to-mass ratio between the adult and child phantoms. This finding was confirmed by comparison with an approximative analytical solution.

1. INTRODUCTION

It has been reported that some people die from heat stroke in summer. The total number of fatalities due to heat stroke in Japan has reached 6,770 from 1968 to 2007 [1]. In addition, there has been some heat waves with some fatalities in different countries. The heat illness is divided into three phases [2, 3]. The mildest form is the heat stress with physical discomfort. Next is the heat exhaustion with dizziness, headache, and dehydration. The most severe stage is the heat stroke characterized by an elevated body core temperature $> 40^{\circ}$C resulting in delirium, convulsions, coma, and death. An excess death rate due to heat illness has been reported among infants and children during heat waves compared with adults [2]. However, it is controversial why only children die from heat stroke [3]. The main reason for this is that it is difficult to experimentally evaluate heat stress in children due to obvious ethical reasons.

There are a large number of studies on the thermoregulatory differences between adults and children [4, 5]. However, information about child thermoregulation and physiological response is not satisfactory. In addition the thermoregulation change from child to adult has not been well clarified. The main differences between the adult and child are morphological and functional. Children have a smaller height and weight in addition to a larger surface area-to-mass ratio than those of adult [4–6]. Associated with the functional aspect of child, the total number of eccrine sweat glands has been found to remain unchanged beyond the age of 2.5 years [7].

In order to clarify the thermophysiological differences between adults and children, Tsuzuki et al. [8, 9] conducted measurements of temperature variation and perspiration in infants (5–10 months old) and their mothers (27–36 years old) in warm and hot environments. She attributed the difference in water loss to the difference in maturity level of the thermoregulation. A straightforward comparison, however, cannot be performed due to physical and physiological differences [8]. Thus, we developed a computational code [10] to follow the temperature elevation and perspiration in numeric human models by comparison with the measured data [8, 9]. We then found that the parameters characterizing the total amount of perspiration were almost

identical between adults and infants, even though their body surface areas are different by three-fold or more.

In addition to higher ambient temperature, the power absorbed in the human due to solar radiation also increases the body temperatures. Thus, a computational approach is needed to obtain some insight on the temperature elevation in the human body exposed to the solar radiation in a hot environment. Note that the necessity to evaluate the temperature elevation in humans due to simultaneous exposure to non-ionizing radiation and heat has been pointed out by an international standardization body [11].

In the present study, we investigated the temperature elevation and perspiration in the adult and child models for simultaneous exposure to the solar radiation and a hot ambient temperature. Different ambient temperatures were considered in the present study. The findings were compared with an analytical solution in order to validate the computational model.

2. MODEL AND METHODS

2.1. Human Body Phantoms

Figure 1 illustrates numeric Japanese male and 3-year-old child phantoms [12]. The adult phantom is segmented into 51 anatomic regions like skin, muscle, bone, brain and heart, with a resolution of 2 mm. The 3-year-old child phantom was developed by applying a free-form deformation algorithm to an adult male phantom [13]. In the deformation, 66 body dimensions were taken into account. The resolution of the child phantom was kept at 2 mm. The height, weight, surface area and surface area-to-mass ratio of the phantoms are listed in Table 1. Note that their surface areas were estimated using the formula [14].

Table 1. Height, weight, surface area, and surface area-to-mass ratio of Japanese phantoms.

	H [m]	W [kg]	S [m^2]	S/W [m^{2}kg^{-1}]
adult male	1.73	65	1.84	0.028
3-year-old	0.90	13	0.56	0.043

2.2. Electromagnetic Analysis

The discretization of computational domain was chosen as 2 mm in order to match the phantom resolution. The FDTD method [15] was

Figure 1. Anatomically based human body phantoms of (a) male adult and (b) 3-year-old child.

used to calculate the power absorption in the human phantoms exposed to the solar radiation. We simplified the solar radiation as a plane wave at 3 GHz due to the following reasons. The primary reason for choosing this frequency is that the weighted moving average of the reflection coefficient [11] in biological tissue for solar spectral irradiance [16] of 35% is comparable to that at 3 GHz of 38%. In addition, the upper frequency at which the FDTD numerical dispersion can be neglected is approximately 3 GHz for biological tissues with the resolution of 2 mm. Note that the penetration depth into the biological tissue (muscle) is about 4 mm. The thermal diffusion length is several centimeters, which is much larger than the penetration depth for the solar radiation of approximately 2 mm [11]. To incorporate the anatomically based phantom into the FDTD method, the electrical constants of the tissues are required. These values were taken from [17]. The validity for this assumption will be discussed later.

2.3. Thermal Analysis Including Thermoregulatory Responses

The temperature elevation in the numeric human phantoms was calculated by solving the bioheat equation [18], which is a model for the thermodynamics inside the human body. The generalized bioheat equation is given as:

$$C(\mathbf{r})\rho(\mathbf{r})\frac{\partial T(\mathbf{r},t)}{\partial t} = \nabla\cdot(K(\mathbf{r})\nabla T(\mathbf{r},t)) + \rho(\mathbf{r})SAR(\mathbf{r}) + A(\mathbf{r},t) - B(\mathbf{r},t))(T(\mathbf{r},t) - T_B(\mathbf{r},t)) \quad (1)$$

where $T(\mathbf{r},t)$ and $T_B(\mathbf{r},t)$ denote the temperatures of tissue and blood, respectively, C is the specific heat of tissue, K is the thermal conductivity of tissue, A is the basal metabolism per unit volume, and B is a term associated with blood perfusion. SAR is the specific absorption rate, suggesting absorption power per unit mass. The boundary condition between air and tissue for Eq. (2) is expressed as:

$$-K(\mathbf{r})\frac{\partial T(\mathbf{r},t)}{\partial n} = H(\mathbf{r})\cdot(T_s(\mathbf{r},t)-T_e(t)) + SW\left(\mathbf{r},T_s(\mathbf{r},t)\right) \quad (2)$$

$$SW\left(\mathbf{r},T_s(\mathbf{r},t)\right) = P_{ins} + SW_{act}\left(\mathbf{r},T_s(\mathbf{r},t)\right) \quad (3)$$

where H, T_s, and T_e denote, respectively, the heat transfer coefficient, the body surface temperature, and the ambient air temperature. The heat transfer coefficient H includes both the convective and radiative heat losses. The evaporative heat loss SW comprises of the heat losses due to perspiration SW_{act} and insensible water loss P_{ins}.

The feature of our computational modeling is that the both the variation in the body core temperature and the temperatures in superficial tissues can be followed, unlike conventional computational schemes. The blood temperature varies according to the following equation, in order to satisfy the first law of thermodynamics [19, 20]:

$$T_B(t) = T_{B0} + \int_t \frac{Q_{BTN}(t)}{C_B\rho_B V_B}dt \quad (4)$$

where Q_{BTN} is the net rate of heat acquisition of blood from body tissues, C_B ($= 4,000\,\mathrm{J/kg^{\circ}C}$) is the specific heat, ρ_B ($= 1,050\,\mathrm{kg/m^3}$) is the mass density, and V_B is the total volume of blood. The blood volume V_B is chosen as 5,000 mL, and 1,000 mL for the adult and child phantoms, respectively [21]. The thermal constants of human tissues and the heat transfer coefficients used in the present study are identical to our previous study [10].

For a temperature elevation above a certain level, the blood perfusion rate was increased in order to carry away excess heat that was produced. The variation of the blood perfusion rate in the skin through vasodilatation is expressed in terms of the temperature elevation at the hypothalamus and the average temperature elevation in the skin [22].

Perspiration for the adult is modeled based on the formulas in [23]. The perspiration coefficients are assumed to depend on the temperature elevation in the skin and hypothalamus:

$$SW(\mathbf{r},t) = \left\{\begin{array}{l}[\alpha_{11}\tanh(\beta_{11}(T_s-T_{s,0})-\beta_{10})+\alpha_{10}](T_s-T_{s,0}) \\ +[\alpha_{21}\tanh(\beta_{21}(T_H-T_{H,0})-\beta_{20})+\alpha_{20}](T_H-T_{H,0})\end{array}\right\} \times\left(0.58\times 4.2\times 10^3+PI\right)/(S\times 60) \quad (5)$$

where S is the surface area of the human body and T_H are the hypothalamus temperature, respectively. Note that in [23] the coefficients of α and β are determined for the average perspiration rate based on measurements [24]. The insensible water loss PI is known to be roughly proportional to the basal metabolic rate: 0.63 g/min for the adult, 0.25 g/min for the child [25]. The point to be stressed here is that a set of parameters of $\alpha_{10} = 1.20$, $\alpha_{11} = 0.80$, $\beta_{10} = 0.19$, $\beta_{11} = 0.59$, $\alpha_{20} = 6.30$, $\alpha_{21} = 5.70$, $\beta_{20} = 1.03$, $\beta_{21} = 1.98$ in Eq. (5) are applicable even to 5–10 month-old infants by comparing with measured and computed results [10]. This implies that the perspiration rate integrated over the body is determined by the body core and skin temperature elevations only, even for different body surface areas.

Computed temperatures in the skin and body core were validated in [10] by comparing with measured temperatures in the skin and body core when changing the ambient temperature [8, 9]. Our computational code has also been validated by comparing measured and computed temperature elevation in rabbits exposed to microwaves [26].

2.4. Exposure Conditions

In order to simulate the solar radiation, the human phantoms were exposed to two plane waves at +45 and −45 degrees from the ground. The former simulates the sunlight directly irradiating the human body and the latter the sunlight reflected from the ground. The power density of the directly incident wave is 1000 W/m^2 based on the average value of solar irradiation tilted 45 degrees from the ground [16]. The power density of reflected wave is 200 W/m^2 based on the ground reflectance of 0.2 [16].

As the thermal exposure condition, firstly, the human is standing in free space at the ambient temperature of 28°C or at the thermo-equilibrium condition. Then, we assumed that the human moves to a place that is exposed to the solar radiation and the ambient temperature of 35, 40, or 45°C. This simultaneous exposure to both the environmental heat and solar radiation is considered as case (i). In addition, solar exposure with a constant air temperature (ii) and the heat exposure without the solar radiation (iii) were considered to clarify the dominant factors influencing core temperature elevation.

3. DERIVATION OF ANALYTICAL SOLUTION

In this section, we derive a formula for estimating the core temperature elevation with the whole-body averaged specific absorption rate (WBA-SAR). Let us consider the heat balance of a biological body as given

in [27–29]:

$$M + P_{RF} - P_t = P_s \tag{6}$$

where M is the rate at which thermal energy is produced through metabolic processes, P_{EM} is the electromagnetic power absorbed in the body, P_t is the rate of heat transfer at the body surface, and P_S is the rate of heat storage in the body. From (6), the total heat balance between the body and air is essential to characterize the core temperature elevation. More specific expression for (6) is given in the following equation based on (2) and (3).

$$\begin{aligned} &\int_o^t \int_V (A(\mathbf{r},\tau) - A_0) dV d\tau + t \int_V \rho(\mathbf{r}) SAR(\mathbf{r}) dV \\ &- \left\{ \int_o^t \int_V H(\mathbf{r},t)(T(\mathbf{r},\tau) - T_e(r)) dV d\tau + \int_o^t \int_S SW(\tau) dS d\tau \right\} \\ = &\int_o^t \int_V \rho(\mathbf{r}) C(\mathbf{r})(T(\mathbf{r},\tau) - T_0(\mathbf{r})) dV d\tau \end{aligned} \tag{7}$$

where T_o and A_o are the thermal steady temperature and basal metabolic rate without exposures. The first term of (7) represents the energy due to the metabolic increment caused by the temperature elevation. In the present study, this term is ignored for simplicity, since this term is much smaller than the amplitudes in the remaining term. Then, we obtained the following equation, as (7) suggests that the SAR and temperature distributions can be assumed to be uniform over the body:

$$\begin{aligned} &(T(\tau) - T_0) \cdot W \cdot C_{WBave} = SAR_{WBave} \cdot W \cdot t \\ &- \int_o^t (T(\tau) - T_0) d\tau \int_S (H_{ave}(t)(T_e(\tau) - T_e(0)) + sw(t)) dS \end{aligned} \tag{8}$$

where $W = \rho_{WBave} \cdot V$ is the weight of the model [kg], SAR_{WBave} is the WBA-SAR [W/kg], H_{ave} is he average heat transfer coefficient between model and ambient air [W/m^2 °C], and C_{WBave} is the mean value of the specific heat [J/kg°C]. $T_e(0)$ is the initial ambient temperature of 28°C and $sw(t)$ is a coefficient identical to $SW(t)$ except that the temperature is assumed to be uniform. Finally, the temperature elevation is obtained as

$$\begin{aligned} T(t) \;=\; T_0 + &\frac{W \cdot SAR_{WBave} + H_{ave}(T_e(\tau) - T_e(0))}{\int_s (H_{ave} + sw(t)) dS} \\ &\left(1 - \exp\left(\frac{\int_s (H_{ave} + sw(t)) dS}{W \cdot C_{WBave}}\right)\right) \end{aligned} \tag{9}$$

where the parameters for Eq. (9) can be found in our previous study.

4. COMPUTATIONAL RESULTS

4.1. Validation

In order to validate our simplification of solar exposure, let us compare the power absorption computed by the FDTD method and an empirical analytical solution. The absorbed power with the FDTD analysis was 320 W and 110 W for the adult and child phantoms, respectively. The power absorption was also evaluated with the following empirical equations:

$$P_{solar} = \int A_{\alpha \cdot B} \cdot S_e dt \tag{10}$$

$$A_{\alpha \cdot B} = \int \gamma(\lambda) \cdot B(\lambda) d\lambda \tag{11}$$

where P_{solar} is the solar power absorbed in the human, $A_{\alpha \cdot B}$ is the absorbed power density, S_e is an effective surface area of the human body [30], γ is rate of absorption to the human body [11] and B is the spectral irradiance. Note that the wavelength of the solar radiation λ from 280 nm to 4000 nm was considered [16]. The validity of the effective surface area of the human has been confirmed in [30] in comparison with measured data. From the Equations (10) and (11), the power absorption was 340 W and 100 W for the adult and child phantoms, respectively. The differences between computed and analytical solution was less than 10%. Thus, the exposure condition simplified as given in Section 2.5 could be reasonable to simulate solar exposure. In the IEEE standard [31], the WBA-SAR is used as a metric for human protection for radio-frequency far-field radiation. The limit is 0.4 W/kg for occupational exposure. In the present case, the WBA-SAR was 5.0 W/kg and 8.5 W/kg for the adult and child phantoms, respectively.

4.2. Computational Results

The time courses of the core and skin temperatures and the cumulative perspiration in the adult and child phantoms are shown in Figs. 2 and 3, respectively. First, let us pay our attention to the case (i). As shown in Fig. 2, the core temperature of the child was comparable to that of the adult. At 1 hour, the core temperature elevations in the adult and child phantoms were 1.34°C and 1.50°C, respectively. From Fig. 3, on the contrary, the cumulative perspiration in the child was much larger than that of the adult. The amount of perspiration in the adult phantom reached 963 g at 1 hour while 2542 g in the child phantom.

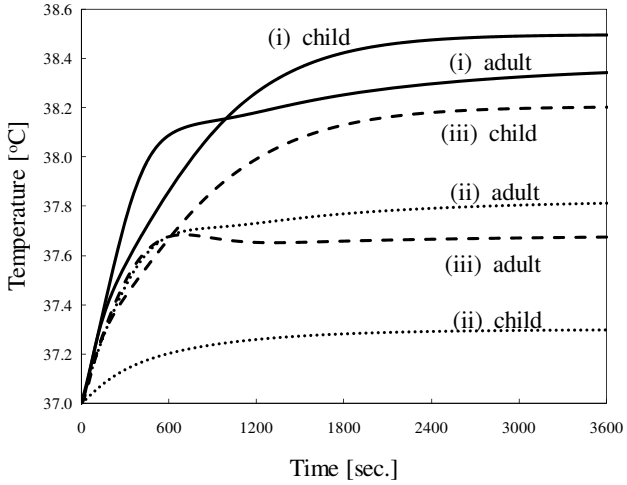

Figure 2. The time course of core temperature in the adult phantom and the child phantom for (i) solar and heat exposure simultaneously, (ii) solar exposure at constant air temperature of 28°C, (iii) heat exposure for the air temperature of 45°C without solar radiation.

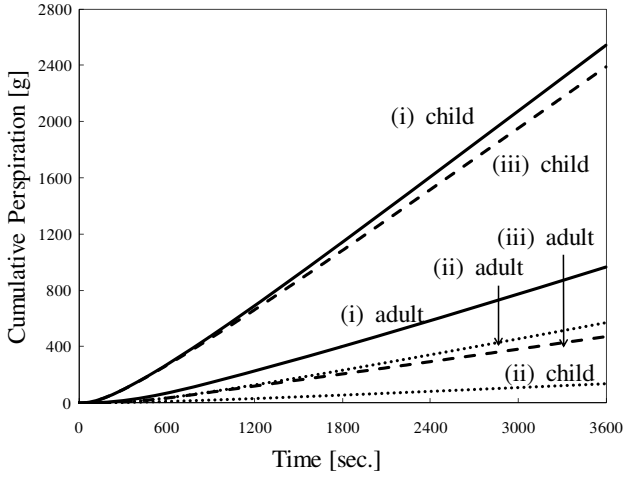

Figure 3. The time courses of cumulative perspiration in the adult and child phantoms for (i) solar and heat exposure simultaneously, (ii) solar exposure at constant air temperature of 28°C, (iii) heat exposure for the air temperature of 45°C without solar radiation.

In order to clarify the reason for the above-mentioned difference, we also computed the core temperature elevation and the cumulative perspiration for two additional cases; (ii) solar exposure at a constant air temperature (28°C) and (iii) exposure to ambient temperature of 45°C without the solar radiation. As shown in Fig. 2, the core temperature elevation was 0.81°C and 0.30°C in the phantom of adult and child, respectively, for the case (ii). From the same figure, the core temperature elevations in the adult and child phantoms were 0.67°C and 1.20°C for the case (iii). The time courses of the cumulative perspiration were similar to those of the core temperature elevation, as is related in Eq. (5). As shown in Fig. 3, the cumulative perspiration at 1 hour was 572 g and 133 g in the adult and child phantoms for the case (ii) while they were 469 g and 2,387 g for the case (iii).

For different ambient temperatures, the time courses of core and skin temperatures and the cumulative perspiration in the adult and child phantoms are shown in Figs. 4 and 5, respectively. As shown in Figs. 4 and 5, the effect of the ambient temperature on both the core temperature elevation the cumulative perspiration was greater in the child than in the adult.

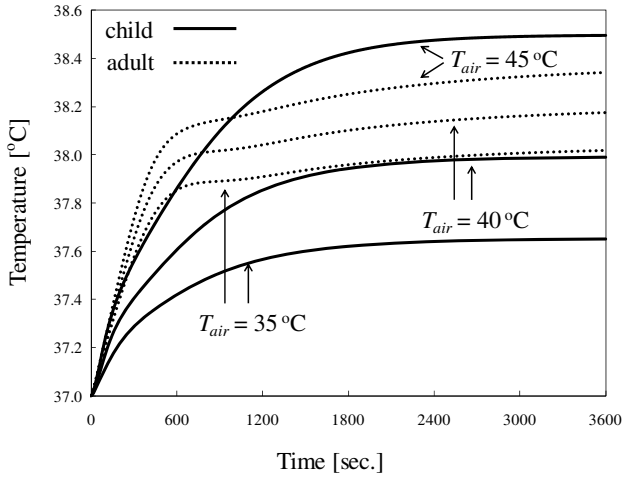

Figure 4. The time course of core temperature in the adult phantom and the child phantom for solar radiation at different ambient temperatures (35, 40, and 45°C).

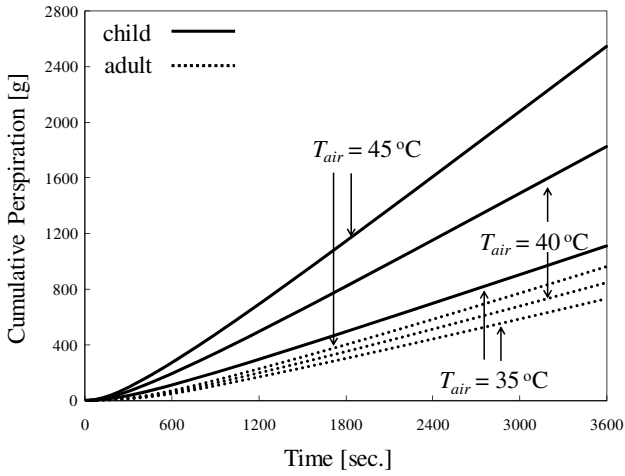

Figure 5. The time courses of cumulative perspiration in the adult and child phantoms for solar radiation at different ambient temperatures (35, 40, and 45°C).

5. DISCUSSION AND SUMMARY

The computed and analytic (9) temperature elevations in the adult phantom for the case (i) with the ambient temperature of 40°C were 1.18°C and 1.04°C, respectively. Similarly, the computed and analytic temperature elevations in the child phantom were 0.99°C and 1.04°C, suggesting the effectiveness of (9) derived in the present study. The formula (9) was originally derived for radio-frequency exposure [29], and then extended to simultaneous exposure to hot air temperature and solar radiation in the present study. Thus, the formula derived herein is applicable to different frequencies including radio-frequency radiation in a hot environment [32–34], for instance, for workers near base station antennas. Also note that the SAR distribution computed with the FDTD method is an approximate one, as the microwave at the frequency of 3 GHz was used instead of sun light. However, the analytic and FDTD temperatures were in good agreement. This is because the total power absorbed in the human is essential rather than the distribution as the WBA-SAR is used as a metric in the safety standard [31].

For the ambient temperature of 45°C, the core temperature elevations due to the solar radiation and the hot-air exposure were comparable in the adult while the latter is dominant in the child. This difference can be explained by the greater surface area-to-mass ratio

in the child compared to the adult, as can be seen from (9). Note that the surface area-to-mass ratio is the dominant factor influencing the core temperature elevation due to the electromagnetic power absorption [29]. Similarly, the energy dissipated via the heat transfer from the surrounding air to the body is proportional to the surface area-to-mass ratio (see Eq. (9)).

By definition, dehydration occurs when the amount of perspiration reaches about 3% of the body weight [1]. For the case (i), the cumulative perspirations in the adult and child phantoms correspond to 1,950 g and 390 g. As shown in Fig. 3, the cumulative perspiration in the child phantom reached 390 g at 14 minutes and those of the adult did not reach to the threshold even at 60 min. In addition to the clear difference in the threshold amount of perspiration, the difference in the perspiration rate should also be noted. As presented in Section 2.4, the perspiration rate integrated over the body is given by the body core and skin temperature elevations only, even for a different body surface area. Due to the difference of the surface area-to-mass ratio, the core and skin temperature elevation become higher, resulting in a larger perspiration rate. The perspiration presented in Figs. 3 and 5 may not be valid at a certain time, especially for the child phantom. The water loss of a child was more than 10% of the body weight at 60 min. and thus the curves may become invalid at a certain time. However, the prime purpose of our study was to obtain insight on the difference in the temperature elevation and perspiration between adults and children for simultaneous exposure of solar radiation and heat. The insight obtained herein will be useful for protection from simultaneous exposures of electromagnetic waves and heat.

ACKNOWLEDGMENT

The authors would like to acknowledge Drs. Soichi Watanabe and Tomoaki Nagaoka for providing their numeric human phantoms.

REFERENCES

1. MOE. Environmental Health Department. Environmental Safety Division 2009 Heat Stoke, Manual of Environmental Health, http://www.env.go.jp/chemi/heat_stroke/manual.html.
2. Danks, D. M., D. W. Webb, and J. Allen, "Heat illness in infants and young children," *Brit. Med. J.*, Vol. 2, 287–293, 1962.
3. McLaren, C., J. Null, and J. Quinn, "Heat stress from enclosed vehicles: moderate air temperature rise in enclosed vehicles," *Pediat.*, Vol. 116, 109–112, 2005.

4. Wagner, J. A., S. Robinson, S. P. Tzankoff, and R. P. Marino, "Heat tolerance and acclimatization to work in the heat in relation to age," *J. Appl. Physiol.*, Vol. 33, 616–622, 1972.
5. Haymes, E. M., E. R. Buskirk, J. L. Hodgson, H. M. Lundegren, and W. C. Nicholas, "Heat tolerance of exercising lean and heavy prepubertal girls," *J. Appl. Physiol.*, Vol. 36, 566–571, 1974.
6. Drinkwater, B. L., I. C. Kupprat, J. E. Denton, J. L. Crist, and S. M. Horvath, "Response of prepubertal girls and college women to work in the heat," *J. Appl. Physiol.*, Vol. 43, 1046–1053, 1977.
7. Kuno, Y., *Human Perspiration*, C. T. Charles, Springfield, IL, 1956.
8. Tsuzuki, K., "Thermoregulation during hot and warm exposures of hot infants compared to their mothers," *Japan. Soc. Home Econ.*, Vol. 49, 409–415, 1998 (in Japanese).
9. Tsuzuki, K., Y. Tochihara, and T. Ohnaka, "Thermoregulation during heat exposure of young children compared to their mothers," *Eur. J. Appl. Physiol.*, Vol. 72, 12–17, 1995.
10. Hirata, A., T. Asano, and O. Fujiwara, "FDTD analysis of body-core temperature elevation in children and adults for whole-body exposure," *Phys. Med. Biol.*, Vol. 53, 5223–5238, 2008.
11. International Commission on Non-Ionizing Radiation Protection (ICNIRP), "ICNIRP statement on far infrared radiation exposure," *Health Phys.*, Vol. 91, 630–645, 2006.
12. Nagaoka, T., S. Watanabe, K. Sakurai, E. Kunieda, M. Taki, and Y. Yamanaka, "Development of realistic high-resolution whole-body voxel models of Japanese adults male and female of average high and weight, and application of models to radio-frequency electromagnetic-field dosimetry," *Phys. Med. Biol.*, Vol. 49, 1–15, 2004.
13. Nagaoka, T., E. Kunieda, and S. Watanabe, "Proportion-corrected scaled voxel models for Japanese children and their application to the numerical dosimetry of specific absorption rate for frequencies from 30 MHz to 3 GHz," *Phys. Med. Biol.*, Vol. 53, 6695–6712, 2008.
14. Fujimoto, S., T. Watanabe, A. Sakamoto, K. Yukawa, and K. Morimoto, "Studies on the physical surface area of Japanese. 18. Calculation formulas in three stages over all ages," *Nippon Eiseigaku Zasshi*, Vol. 23, 443–450, 1968 (in Japanese).
15. Taflove, A. and S. Hagness, *Computational Electrodynamics: The Finite-difference Time-domain Method*, 3rd edition, Artech House, Norwood, MA, 2003.

16. ASTM G173-03. Standard Tables for Reference Solar Spectral Irradiances: Direct Normal and Hemispherical on 37° Tilted Surfaces, 2008.
17. Gabriel, C., "Compilation of the dielectric properties of body tissues at RF and microwave frequencies," Final Tech. Rep. Occupational and Environmental Health Directorate, AL/OE-TR-1996-0037, RFR Division, Brooks Air Force Base, TX, 1996.
18. Pennes, H. H., "Analysis of tissue and arterial blood temperatures in resting forearm," *J. Appl. Physiol.*, Vol. 1, 93–122, 1948.
19. Bernardi, P., M. Cavagnaro, S. Pisa, and E. Piuzzi, "Specific absorption rate and temperature elevation in a subject exposed in the far-field of radio-frequency sources operating in the 10-900-MHz range," *IEEE Trans. Biomed. Eng.*, Vol. 50, 295–304, 2003.
20. Hirata, A. and O. Fujiwara, "Modeling core temperature variation in the bioheat equation and its application to temperature analysis due to RF exposure," *Phys. Med. Biol.*, Vol. 54, N186–N196, 2009.
21. International Commission on Radiological Protection (ICRP), Report of the Task Group on Reference Man Vol. 23, Pergamon Press, Oxford, 1975.
22. Hoque, M. and O. P. Gandhi, "Temperature distribution in the human leg for VLF-VHF exposure at the ANSI recommended safety levels," *IEEE Trans. Biomed. Eng.*, Vol. 35, 442–449, 1988.
23. Fiala, D., K. J. Lomas, and M. Stohrer, "Computer prediction of human thermoregulation and temperature responses to a wide range of environmental conditions," *Int. J. Biometeorol.*, Vol. 45, 143–159, 2001.
24. Stolwijk, J. A. J., *A Mathematical Model of Physiological Temperature Regulation in Man*, NASA (CR-1855), Washington, DC, 1971.
25. Fanaroff, A. A., M. Wald, H. S. Gruber, and M. H. Klaus, "Insensible water loss in low birth weight infants," *Pediatrics*, Vol. 50, 236–245, 1972.
26. Hirata, A., H. Sugiyama, M. Kojima, H. Kawai, Y. Yamashiro, S. Watanabe, H. Sasaki, and O. Fujiwara, "Acute dosimetry and estimate of thresholds inducing behavioral sign of thermal stress for 2.45-GHz microwave exposure in rabbits," *IEEE Trans. Biomed. Eng.*, Vol. 57, No. 5, 1234–1242, 2010.
27. Adair, E. R. and D. R. Black, "Thermoregulatory responses to RF energy absorption," *Bioelectromagnetics Suppl.*, Vol. 6, S17–S38, 2003.

28. Ebert, S., S. J. Eom, J. Schuderer, U. Spostel, T. Tillmann, C. Dasenbrock, and N. Kuster, "Response, thermal regulatory threshold of restrained RF-exposed mice at 905 MHz," *Phys. Med. Biol.*, Vol. 50, 5203–5215, 2005.
29. Hirata, A., H. Sugiyama, and O. Fujiwara, "Estimation of core temperature elevation in humans and animals for whole-body averaged SAR," *Progress In Electromagnetics Research*, Vol. 99, 53–70, 2009.
30. Kubaha, K., D. Fiala, J. Toftum, and A. H. Taki, "Human projected area factors for detailed direct and diffuse solar radiation analysis," *Int. J. Bio.*, Vol. 49, 113–129, 2004.
31. IEEE, "IEEE standard for safety levels with respect to human exposure to radio frequency electromagnetic fields, 3 kHz to 300 GHz," C95-1, 2005.
32. Liu, Y., Z. Liang, and Z. Yang, "Computation of electromagnetic dosimetry for human body using parallel FDTD algorithm combined with interpolation technique," *Progress In Electromagnetics Research*, Vol. 82, 95–107, 2008.
33. Lopez-Martin, E., J. C. Bregains, F. J. Jorge-Barreiro, J. L. Sebastian-Franco, E. Moreno-Piquero, and F. Ares-Pena, "An experimental set-up for measurement of the power absorbed from 900 MHz GSM standing waves by small animals, illustrated by application to picrotoxin-treated rats," *Progress In Electromagnetics Research*, Vol. 87, 149–165, 2008.
34. Mohsin, S. A., N. M. Sheikh, and U. Saeed, "MRI induced heating of deep brain stimulation leads: Effect of the air-tissue interface," *Progress In Electromagnetics Research*, Vol. 83, 81–91, 2008.